This journal is © The Royal Society of Chemistry 2015

Supplementary Information:

Mapping surface tension induced meniscus with application to tensiometry and refractometry

Avanish Mishra,[a] Varun Kulkarni,[b] Jian-Wei Khor [a] and Steve Wereley*[a]

[a] Birck Nanotechnology Centre, School of Mechanical Engineering, Purdue University, West Lafayette, IN – 47907

[b] Maurice J. Zucrow Laboratories, School of Mechanical Engineering, Purdue University, West Lafayette, IN – 47907

1. Refraction at the inclined plate

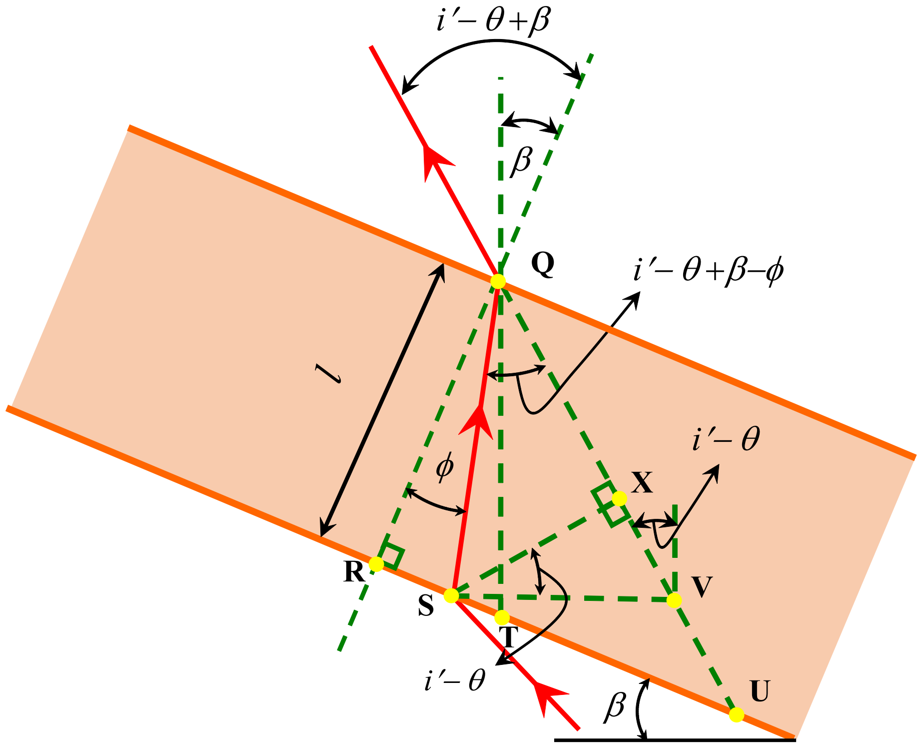

Fig. S1 Optics inside the inclined flat plate. The solid red line corresponds to the incident/refracted ray. The green dashed lines are construction lines used to determine various geometrical distances.

In the ensuing section, we derive an analytical expression for MM^o, the displacement of the point **M** due to refraction at the inclined glass plate. To begin with we describe various quantities as indicated in Fig. S1. Point **S** corresponds to the location where the incident ray from the point **M** hits the flat plate. Point **Q** is where the refracted ray exits the flat plate. Thus, QS is the distance traversed along its path. l (= QR) is the thickness of the flat plate in the incidence plane. As mentioned before, β is the angle of inclination of the plate. i', is the angle of incidence at the meniscus which is refracted at an angle i. θ, is the angle of the surface slope which is, $\partial h / \partial x = -tan\theta$. In terms of the above quantities, we note that the angle of refraction of the emerging refracted ray is given by, $i' - \theta + \beta$ with respect to the surface normal of the inclined plate. It is important to recognize that SV in Fig. S1 is same as MM^o.

First we need to estimate the angle ϕ. From the Snell Descartes law, with n' and n_g representing the refractive indices of the liquid and glass medium, we obtain,

$$\frac{n_g}{n'} = \frac{sin(i' - \theta + \beta)}{sin\phi}$$ * MERGEFORMAT (1)

Since, i' and θ is very small (weak slope and paraxial approximation), eqn (1) reduces to,

$$\therefore \frac{n_g}{n'} = \frac{sin\beta}{sin\phi}$$ * MERGEFORMAT (2)

From eqn (2), we may derive an expression for ϕ as

$$\phi = \sin^{-1}\left(\frac{n' sin\beta}{n_g}\right)$$ * MERGEFORMAT (3)

In order to determine SV, we would need to calculate a few intermediate quantities which are described in the steps below. We first consider right angled Δ QRS. Here

$$QS = \frac{l}{\cos\phi}$$ * MERGEFORMAT (4)

Similarly, from Δ QSX and Δ SVX we have,

$$SX = \left(\frac{l}{cos\phi}\right) sin(i' - \theta + \beta - \phi)$$ * MERGEFORMAT (5)

$$\text{and, } SV = \left[\frac{l}{cos\,\phi}\right]\left[\frac{sin\left(i'-\theta+\beta-\phi\right)}{cos\left(i'-\theta\right)}\right] \quad \text{* MERGEFORMAT (6)}$$

Once again for small i' and θ we have

$$SV = \left(\frac{l}{cos\,\phi}\right) sin\left(\beta-\phi\right) \quad \text{* MERGEFORMAT (7)}$$

2. Representation of $\hat{\boldsymbol{n}}$ in terms of $\hat{\boldsymbol{s}}$ and $\mathbf{CM''}$

The vector $\hat{\boldsymbol{n}}$ can be expressed using $\hat{\boldsymbol{s}}$ and $\mathbf{CM''}$ as,

$$\hat{\boldsymbol{n}} = a\hat{\boldsymbol{s}} + b\frac{\mathbf{CM''}}{\left|\mathbf{CM''}\right|} \quad \text{* MERGEFORMAT (8)}$$

The coefficients, a and b can be determined by the following geometric relations

$$\hat{\boldsymbol{n}} \cdot \hat{\boldsymbol{s}} = \text{-}\sin\theta \quad \text{* MERGEFORMAT (9)}$$

$$\hat{\boldsymbol{n}} \cdot \frac{\mathbf{CM''}}{\left|\mathbf{CM''}\right|} = \text{-}\cos i \quad \text{* MERGEFORMAT (10)}$$

$$\hat{\mathbf{s}} \cdot \frac{\mathbf{CM''}}{\left|\mathbf{CM''}\right|} = \sin(i\,\text{-}\,\theta) \quad \text{* MERGEFORMAT (11)}$$

Using the above geometric relations, we get

$$\hat{\boldsymbol{n}} = \frac{\cos i \sin\left(i-\theta\right) - \sin\theta}{\cos^2\left(i-\theta\right)}\hat{\boldsymbol{s}} + \frac{\sin\theta\sin\left(i-\theta\right) - \cos i}{\cos^2\left(i-\theta\right)}\frac{\mathbf{CM''}}{\left|\mathbf{CM''}\right|} \quad \text{* MERGEFORMAT}$$

(12)

Using the weak slope and paraxial approximations, we get

$$\hat{\boldsymbol{n}} = i\hat{\boldsymbol{s}} - \frac{\mathbf{CM''}}{\left|\mathbf{CM''}\right|} \quad \text{* MERGEFORMAT (13)}$$

3. Derivation of $\mathbf{M^{o}M''}$

Considering $\Delta\,\mathrm{IKM}$ and $\Delta\,\mathrm{IKM''}$ in the incidence plane (as shown in Fig. 3 in the manuscript), we obtain

$$\mathbf{M^oM''} = \mathbf{KM''} - \mathbf{KM^o}$$ * MERGEFORMAT (14)

$$\mathbf{KM''} = h_p(i-\theta)\hat{\mathbf{s}}$$ * MERGEFORMAT (15)

$$\mathbf{KM^o} = h_{\mathrm{p}}(i'-\theta)\hat{\mathbf{s}}$$ * MERGEFORMAT (16)

$$\mathbf{M^oM''} = \alpha h_{\mathrm{p}} i\hat{\mathbf{s}}$$ * MERGEFORMAT (17)

4. Theoretical meniscus profile on an inclined plate

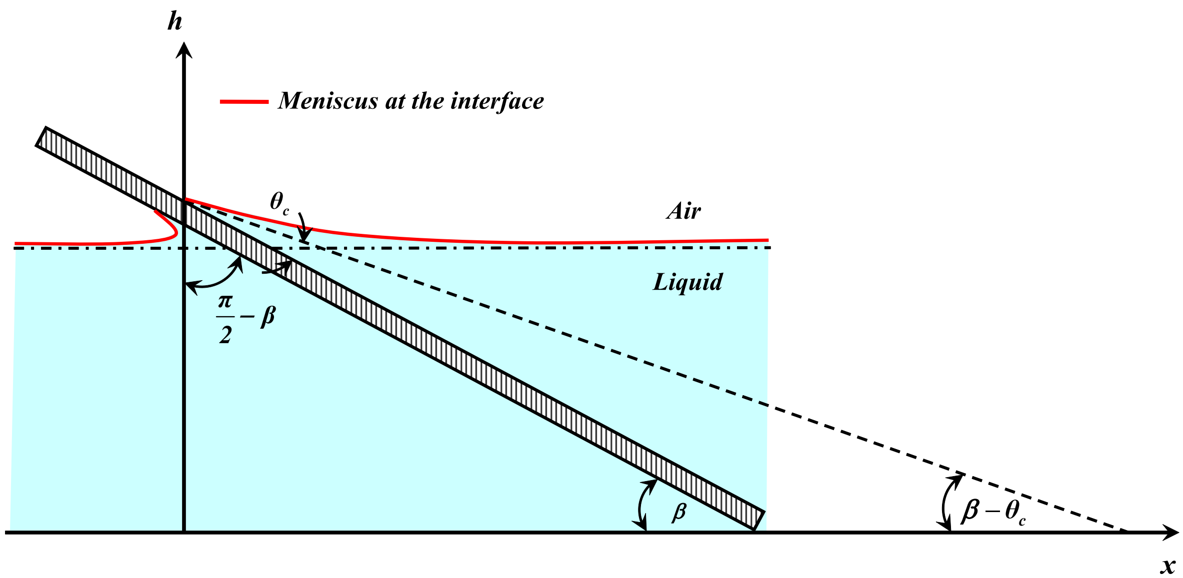

Fig. S2 Sketch of inclined flat plate liquid meniscus and coordinate axes. Shaded rectangle in the figure corresponds to the flat plate.

To obtain a theoretical expression for the meniscus, the Young-Laplace equation is solved in Cartesian coordinates[1]. The governing equation reads as

$$\frac{d^2h}{dx^2}=\left(\frac{\rho g}{\sigma}h\right)\left[1+\left(\frac{dh}{dx}\right)^2\right]^{3/2}$$ * MERGEFORMAT (18)

subject to the boundary conditions,

$$\frac{dh}{dx}=-tan\,\alpha \quad \text{at} \quad x=0$$ * MERGEFORMAT (19)

$$h\rightarrow 0 \quad \text{at} \quad x\rightarrow\infty$$ * MERGEFORMAT (20)

Here, $\alpha=\beta-\theta_c$, where θ_c is the contact angle between the liquid and gas as shown in Fig. S2. In the case where the slope is slender *i.e*. dh/dx << 1 eqn (18) transforms to

$$\frac{d^2h}{dx^2}=\left(\frac{\rho g}{\sigma}h\right)$$ * MERGEFORMAT (21)

Solving eqn (21) using the boundary conditions specified in eqn (19) and eqn (20), we obtain eqn (22), the expression for the meniscus height (*h*) as a function of the distance (*x*)

$$\frac{h}{l_c}=tan(\alpha)e^{-x/l_c}$$ * MERGEFORMAT (22)

where l_c is the capillary length, $\sqrt{\sigma/\rho g}$.

5. Materials and Methods

A glass container of 15 cm diameter and 75 mm height was used for experiments. The bottom surface of the container was optically flat. Images were captured using an 8 bit Nikon DS-fi1 camera equipped with a 40 mm Micro-Nikkor lens. The f-stop was kept at 22 in all the measurements. Camera CCD sensor is 8.70 mm wide and 6.53 mm high. Physical pixel size is 3.4 µm. For background illumination, we used a 100W Nikon halogen lamp (Fig. S3). It is important note that any uniform light source will be sufficient for background illumination. A glass diffuser was utilized as a background pattern. A distribution of diameter of dots is being shown in Fig. S4. Though not used in this work, a high resolution dot pattern printed with a photomask printer on a transparent sheet will also be an excellent choice for a background pattern. In the current experiments, images were acquired using Nikon NIS-Elements F 3.0 software. The original images were recorded with a resolution of 2560×1920 pixel^2 but for analysis, we decided to work with a subset of the area in the original image (208×1232 pixel^2) as it is sufficient for finding surface tension and contact angle. A 0.15 mm thick glass plate was used as the inclined flat plate. Before use, glass plate was solvent cleaned by ultrasonication for 3 minutes each in acetone, isopropanol and methanol. Subsequently, the plate was carefully washed with distilled water, blow dried with nitrogen gas, and plasma treated to ensure uniform wetting. Before use, it was microscopically inspected for any dirt or impurity on the surface. The angle of the inclined plate was directly measured by a degree indicator on the rotation stage. We also used a camera positioned in side view to confirm the angle of the plate. Public domain image processing software ImageJ was used to measure the angle of the plate from the recorded images. All the experiments were performed at a temperature of 293±1 K. For finding surface tension, refractive index and contact angle, experiments were repeated ten times for each liquid and one standard deviation of the data was used as a measure of uncertainty in the measured values.

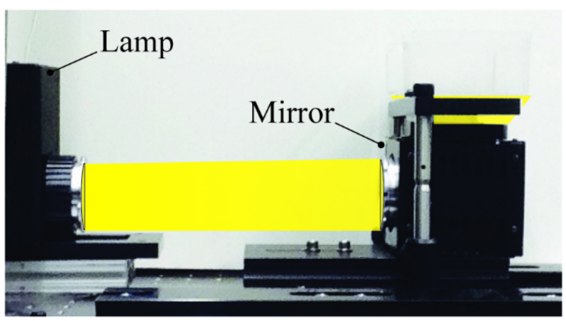

Fig. S3 Background illumination setup. A 45° mirror reflects light from the lamp in to the glass container.

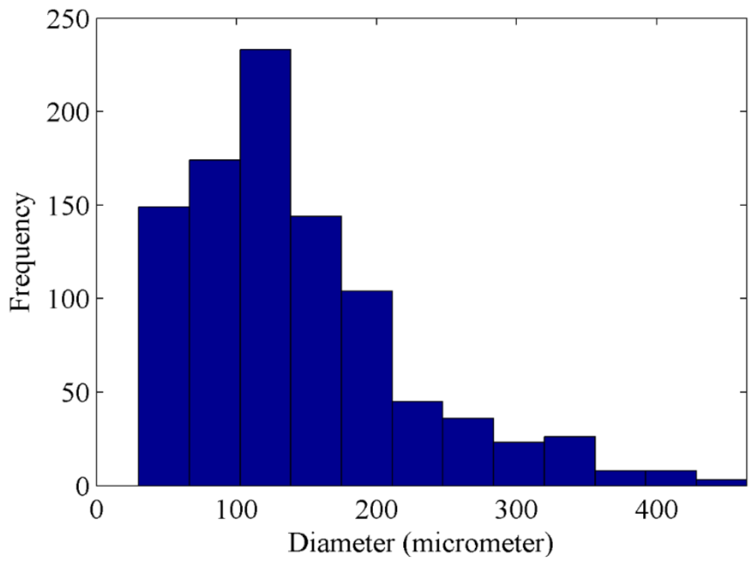

Fig. S4 Distribution of size of dots

6. PIV Processing Parameters

To evaluate the displacement field, first the images were preprocessed with a local low pass filter. It removes any variation in the background intensity by subtracting the local background from the original image. We then performed cross-correlation in multi pass mode with decreasing window sizes. The cross correlation started with 50% overlapping windows of 64×64 pixel^2 and concluded with a window size of 16×16 pixel^2 with 50% overlap. Multiple iterations were performed for each window size. For starting window size of 64×64 pixel^2, 3 iterations were performed. For final window size of 16×16 pixel^2, 5 iterations were performed. The computed vectors were post-processed for removal of outliers. During post-processing, vectors with peak ratio less than 1.3 were removed. A 4-pass regional median filter with 'strongly remove and iteratively replace' option was utilized to eliminate groups of spurious vectors. For each vector, median filter computes the median of 8 surrounding vectors and keeps the vector if it falls within the range of median vector±(2×root mean square (rms) of neighbor vectors). In second pass, vectors which do not have 3 or more neighboring vectors left from previous pass were removed. In third pass all the good vectors which fall in the range of median vector±(3×rms of neighbor vectors) were reinserted. Finally, in fourth pass groups with less than 5 vectors were removed. In vector post-processing, after removal of spurious vectors, empty spaces were filled with new vectors by interpolation. It is important to mention that less than 1.5 % vectors were filled by interpolation in all the cases. We used the PIVMat® toolbox developed by Moisy et al.[2] for surface height reconstruction. For fitting, we used the nonlinear least squares method with the robust option in MATLAB®.

References

1 G. K. Batchelor, *An Introduction to Fluid Dynamics*, Cambridge University Press, 2000.

2 F. Moisy, M. Rabaud and K. Salsac, *Exp. Fluids*, 2009, **46**, 1021–1036.